Chinese Journal of Natural Medicines

New phenylbutenoids and terpene glycosides from *Ginkgo biloba* leaves

Ze-Shi SUN, Shan LIN, Zhi-Li WU, Hong-Yuan DONG, Xi-Ke XU, Hui-Liang LI, Jin-Xin WANG

Citation: Ze-Shi SUN, Shan LIN, Zhi-Li WU, Hong-Yuan DONG, Xi-Ke XU, Hui-Liang LI, Jin-Xin WANG, New phenylbutenoids and terpene glycosides from *Ginkgo biloba* leaves, Chinese Journal of Natural Medicines, 2024, 22(2), 1-10. doi: 10.1016/S1875-5364(23)60414-5.

View online: https://doi.org/10.1016/S1875-5364(23)60414-5

Available online at www.sciencedirect.com
ScienceDirect
Chinese Journal of Natural Medicines 2024, **22**(2): 161-170
doi: 10.1016/S1875-5364(24)60588-1
Chinese Journal of Natural Medicines

•Original article•

New phenylbutenoids and terpene glycosides from *Ginkgo biloba* leaves

SUN Zeshi[1], LIN Shan[2], WU Zhi-Li[1], DONG Hong-Yuan[1], XU Xi-Ke[1], LI Hui-Liang[1*], WANG Jinxin[1*]

[1] *School of Pharmacy, Second Military Medical University, Shanghai 200433, China;*
[2] *State Key Laboratory of New Drug and Pharmaceutical Process, Shanghai Institute of Pharmaceutical Industry, China State Institute of Pharmaceutical Industry, Shanghai 201203, China*

Available online 20 Feb., 2024

[ABSTRACT] Our continued works on the chemical constituents of *Ginkgo biloba* (*G. biloba*) leaves has led to the isolation of two novel phenylbutenoids (**1**, **2**), along with five previously unidentified terpene glycosides (**3**−**7**). Among them, compounds **1** and **2** represent unique (*Z*)-phenylbutenoids, **3**−**6** are megastigmane glycosides, and **7** is identified as a rare bilobanone glycoside (Fig. 1). This study marks the first reported isolation of phenylbutenoid and bilobanone glycoside from *G. biloba*. The chemical structures of these compounds were elucidated through extensive spectroscopic analysis, including HR-ESI-MS and various 1D and 2D NMR experiments. Furthermore, the absolute configurations of these molecules were determined using Mosher's method, ECD experiments, and Cu-Kα X-ray crystallographic analyses.

[KEY WORDS] *Ginkgo biloba*; Phenylbutenoid; Megastigmane glycoside; Bilobanone glycoside.
[CLC Number] R284.1 **[Document code]** A **[Article ID]** 2095-6975(2024)02-0161-10

Introduction

Ginkgo biloba L. (*G. biloba* L.), a perennial deciduous tree belonging to the genus *Ginkgo* in the family *Ginkgoaceae*, stands as a unique plant in China and a rare remnant of the Mesozoic Era [1]. Recognized as one of the world's most ancient plants, it has a broad distribution in East Asia, Europe, America, and other regions [2, 3]. *G. biloba* is distinguished by its diverse array of compounds with unique structures, including flavonoids, terpenoids, alkylphenols, alkylphenolic acids, carboxylic acids, lignans, proanthocyanidins, and polyprenols [4-10]. These compounds have exhibited remarkable effects, such as antioxidation, anti-inflammation, circulation improvement, anti-platelet aggregation, neuroprotection, anti-tumor activity, and anti-radiation properties [11-16]. As one of the top-selling herbal products, the extract of the *G. biloba* leaf extract (GBE) has gained widespread use in the pharmaceutical, health food, and cosmetic industries worldwide, achieving over $10 billion in sales since 2017 [16].

Although the standardized GBE preparation, EGb761, has received approval for marketing as a treatment for asthma, bronchitis, ischemia, arteriosclerosis, and rheumatism [17], only 30% of its ingredients are characterized (24% ginkgo flavonoids and 6% terpene lactones), leaving the structures and properties of the remaining constituents largely undefined. Investigating the chemical composition of GBE, along with the bioactivity and cytotoxicity of its components (especially for the *G. biloba* injection), is crucial for both fundamental research and clinical applications. Our previous phytochemical investigation into the characterized ingredients of GBE led to the discovery of a new bilobalide isomer and two novel flavonol glycosides [8]. In our continued efforts to investigate chemical constituents from the GBE, two phenylbutenoids, four megastigmane glycosides, and one bilobanone glycoside were isolated from the plant. This paper reports on the isolation, structural identification, and cytotoxicity evaluation of these newly identified compounds.

[Received on] 17-Aug.-2023
[Research funding] This work was supported by the National Natural Science Foundation of China (Nos. 82141203, 82003624, 82004003, and 82004215), the Science and Technology Commission of Shanghai Municipality (Nos. 20YF1458700 and 20YF1459000), the Innovation Team and Talents Cultivation Program of National Administration of Traditional Chinese Medicine (No. ZYYCXTDD-202004), and Shanghai Frontiers Science Center of TCM Chemical Biology, Shanghai Engineering Research Center for the Preparation of Bioactive Natural Products (No. 16DZ2280200).
[*Corresponding author] E-mails: faranli@hotmail.com (LI Hui-Liang); jxwang2013@126.com (WANG Jinxin)
These authors have no conflict of interest to declare.

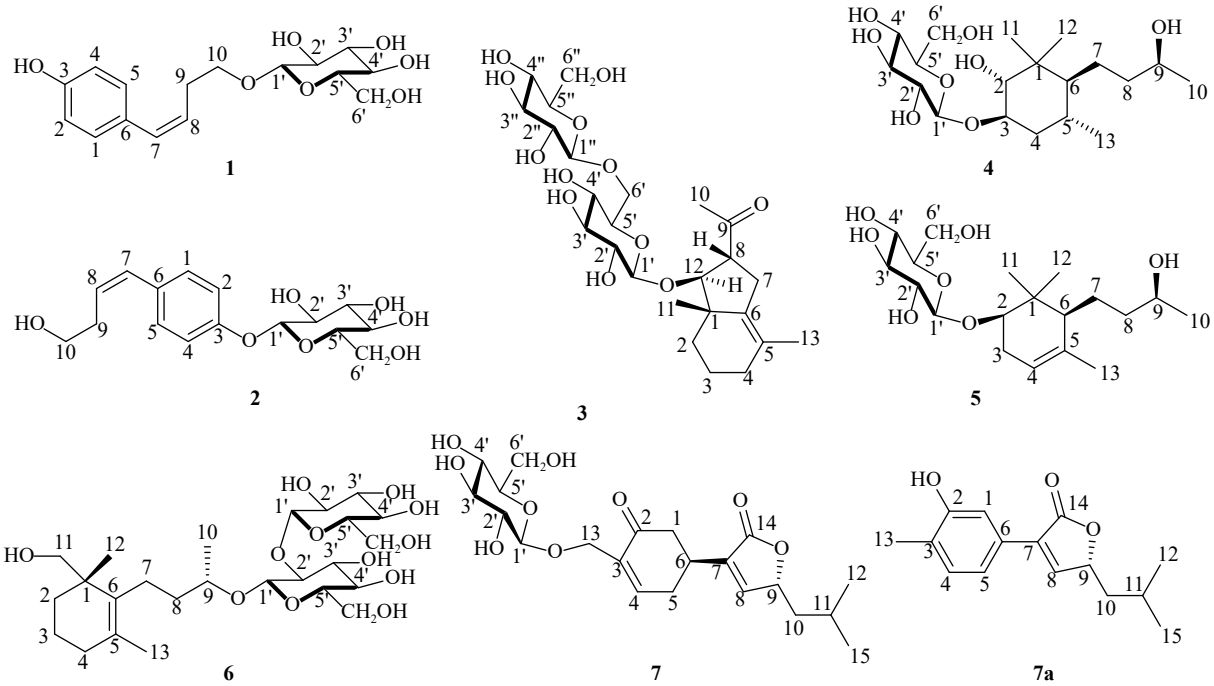

Fig. 1 Chemical structures of 1−7 and 7a.

Results and Discussion

Compound **1** was obtained as needle crystals (H_2O−MeOH). Its molecular formula was determined as $C_{16}H_{22}O_7$ based on positive High-Resolution Electrospray Ionization Mass Spectrometry (HR-ESI-MS) at *m/z* 349.1264 ([M + Na]$^+$, Calcd. 349.1258), indicating six degrees of unsaturation.

The ^{1}H Nuclear Magnetic Resonance (NMR) spectrum (Table 1) of **1** revealed resonant signals corresponding to a para-substituted phenyl group [δ_H 6.83 (2H, d, J = 8.57 Hz), 7.23 (2H, d, J = 8.57 Hz)] and an olefin group [δ_H 5.63 (1H, dt, J = 11.76, 7.20, 4.54 Hz), 6.45 (1H, d, J = 11.76 Hz)]. The ^{13}C NMR spectrum of **1** indicated the presence of 16 carbons, categorized into three methylenes, seven methines (including two sp^2 carbons at δ_C 127.5 and 131.1), and a phenyl group (δ_C 131.2, 116.1, 155.9, 116.1, 131.2 and 130.6). Particularly, four signals for six aromatic carbons, in conjunction with Heteronuclear Multiple Bond Correlations (HMBCs) (Fig. 2) of H-2 (δ_H 6.83) and H-4 (δ_H 6.83) with C-3 (δ_C 155.9), confirmed the presence of a para-substituted phenol group. The presence of one anomeric carbon (δ_C 103.6) and five oxygenated carbons (δ_C 74.4, 77.2, 70.9, 77.2, 62.0) indicated a glucose moiety. The remaining four carbons were inferred to form a butene unit. The ^{1}H-^{1}H Correlation Spectroscopy (COSY) correlations (Fig. 2) of H-7/H-8/H-9/H-10, along with the HMBCs of H-9 (δ_H 2.64) with C-7 (δ_C 131.1) and C-8 (δ_C 127.5), delineated this butene as 1-butylene. Furthermore, the HMBCs of H-8 (δ_H 5.63) with C-6 (δ_C 130.6) and H-7 (δ_H 6.45) with C-1 (δ_C 131.2) and C-5 (δ_C 131.2) suggested the attachment of the butene to the para-substituted phenol at C-6 and C-7. The anomeric proton signal of H-1' (δ_H 4.38)

Table 1 ^{1}H NMR (500 MHz, CD_3OD, J in Hz) and ^{13}C NMR (125 MHz, CD_3OD) spectroscopic data for compounds 1 and 2.

No.	1		2	
	δ_H (J in Hz)	δ_C	δ_H (J in Hz)	δ_C
1	7.22, d (8.57)	131.2	7.31, d (8.71)	131.1
2	6.83, d (8.57)	116.1	7.09, d (8.75)	117.4
3	-	155.9	-	156.7
4	6.83, d (8.57)	116.1	7.09, d (8.75)	117.4
5	7.22, d (8.57)	131.2	7.31, d (8.71)	131.1
6	-	130.6	-	133.3
7	6.45, d (11.76)	131.1	6.50, d (11.71)	130.9
8	5.63, dt (11.76, 7.20, 4.54)	127.5	5.67, dt (11.71, 7.23, 4.44)	129.1
9	2.64, m	29.8	2.54, m	32.3
10	3.97, m, 3.72, m	70.7	3.67, m	62.4
1'	4.38, d (7.97)	103.6	5.04, d (7.46)	101.5
2'	3.18−3.44, m (overlap)	74.4	3.45−3.57, m (overlap)	74.2
3'	3.18−3.44, m (overlap)	77.2	3.45−3.57, m (overlap)	77.3
4'	3.18−3.44, m (overlap)	70.9	3.45−3.57, m (overlap)	70.6
5'	3.18−3.44, m (overlap)	77.2	3.45−3.57, m (overlap)	76.9
6'	3.68, m, 3.85, d (12.10)	62.0	3.73, m, 3.90, m	61.8

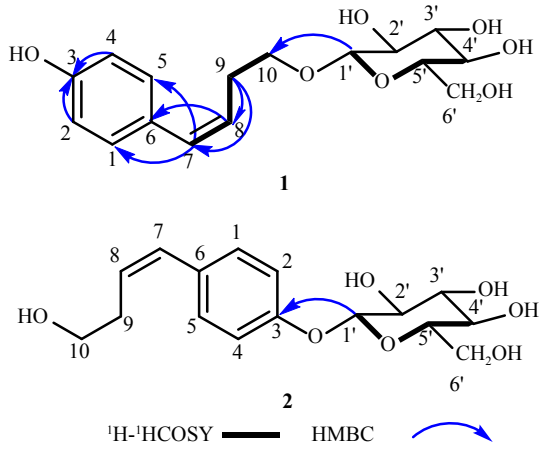

Fig. 2 Selected NMR correlations of 1 and 2.

showed a correlation with the carbon signal of C-10 (δ_C 70.7), suggesting the glycosylation at C-10. The coupling constant of the anomeric proton H-1' (J = 7.97 Hz) implied a *β*-configuration for the anomeric carbon. Furthermore, the formation of white needle crystals in an H_2O–MeOH solution and the presence of a *cis*-olefin group, along with the configuration of **1**, was unambiguously confirmed by Cu-Kα X-ray crystallographic analysis (Fig. 3).

Compound **2** was isolated as needle crystals (H_2O–MeOH). Its molecular formula was determined as $C_{16}H_{22}O_7$, as evidenced by positive HR-ESI-MS data at *m/z* 349.1257 ($[M + Na]^+$, Calcd. 349.1258), indicating six degrees of unsaturation.

The ^1H and ^{13}C NMR spectra of **2** (Table 1) closely resembled those of **1**. The major difference was the presence of a hydroxyl group carbon (δ_C 62.4, C-10) in **2** that replaced the oxygen-bearing carbon (δ_C 70.7, C-10) in **1**. This observation was supported by the HMBC of anomeric proton H-1' (δ_H 5.04) with the carbon C-3 (δ_C 156.7). The planar structure of **2** was elucidated through a comprehensive analysis of ^1H-^1H COSY, HSQC, and HMBC spectra (Fig. 2). The configuration of **2** was determined by Cu-Kα X-ray crystallographic analysis (Fig. 4).

Compound **3**, $[\alpha]_D^{25}$ −47.33 (*c* 0.08, CH_3OH), was isolated as a white powder (MeOH). Its molecular formula was

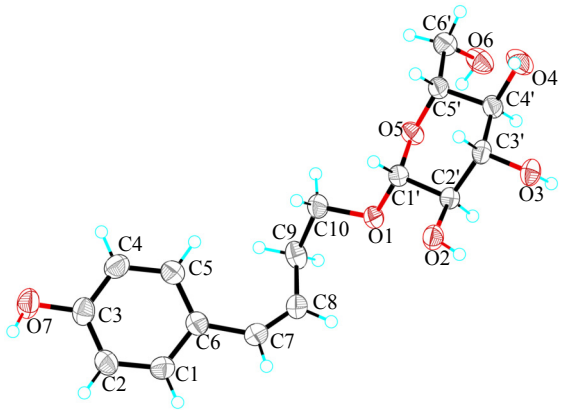

Fig. 3 X-ray crystallographic structure of 1.

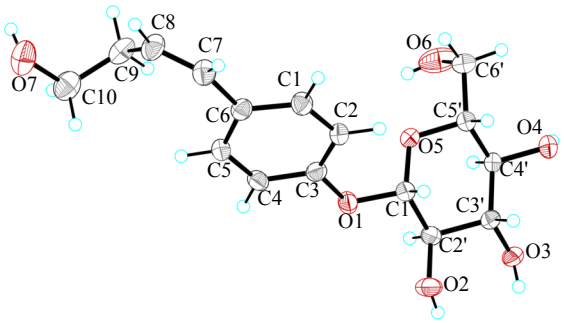

Fig. 4 X-ray crystallographic structure of 2.

determined as $C_{25}H_{40}O_{12}$, as indicated by positive HR-ESI-MS data at *m/z* 555.2411 ($[M + Na]^+$, Calcd. 555.2412), suggesting six degrees of unsaturation.

The structure of **3** was constructed by the analyses of its ^1H NMR and ^{13}C NMR spectra, complemented by ^1H-^1H COSY and HMBC spectra. The one-dimensional (1D) NMR spectrum of **3** (Table 2) revealed 25 carbon signals, categorized into three methyl groups, six methylene groups (including one hydroxyl methylene at δ_C 61.3, and one oxygenated methylene at δ_C 68.0), twelve methines (including six hydroxyl methines at δ_C 73.8, 69.8, 75.1, 73.7, 76.4 and 70.1 and five oxygenated methines at δ_C 91.0, 103.6, 76.4, 103.0 and 76.4), and four quaternary carbons (containing three sp^2 carbons at δ_C 133.3, 125.8 and 213.8). Furthermore, the presence of an acetyl group in **3** was inferred from resonance signals at δ_C 213.8, 30.3, and δ_H 2.30 (3H, s) in the NMR spectra. Based on these observations, it was deduced that compound **3** should contain two glucose moieties, with the remaining 13 carbon resonances indicating the presence of a megastigmane unit.

The planar structure of **3** was further established by comprehensive analyses of its ^1H-^1H COSY and HMBC spectra (Fig. 5). Interpretation of the ^1H-^1H COSY and HSQC spectra revealed the presence of two partial structures, "C-2/C-3/C-4" and "C-7/C-8/C-12". These partial structures were interconnected *via* a quaternary carbon (C-1), as evidenced by the HMBCs of H-11 (δ_H 1.03, 3H) with C-6 (δ_C 133.3), C-2 (δ_C 34.6), C-1 (δ_C 44.5), and C-12 (δ_C 91.0), suggesting the linkage of C-11 and C-6 to C-1. Key HMBCs of H-4 (δ_H 1.69, 1.92), H-3 (δ_H 1.70, 1.93), and H-13 (δ_H 1.53) with C-5 (δ_C 125.8) were observed, indicating that C-4 and C-13 were connected to C-5. These correlations, combined with HMBCs of H-7 (δ_H 2.32, 2.57) with C-6 (δ_C 133.3) and C-5 (δ_C 125.8), revealed that the megastigmane aglycone of **3** consists of two rings. Meanwhile, the acetyl group was determined to be attached to C-8 based on the HMBCs of H-10 (δ_H 2.30, 3H, s) with C-8 (δ_C 53.0). Finally, the HMBCs of H-1' (δ_H 4.25) with C-12 (δ_C 91.0) as well as H-1" (δ_H 4.29) with C-6' (δ_C 68.0) indicated that a glucose unit was linked to the 12-hydroxy group of the megastigmane unit, and a second glucose unit was attached to the 6'-hydroxy group of the first glucose. Therefore, the planar structure of **3** was elucidated, as depicted in Fig. 1.

Table 2 ^{1}H NMR (500 MHz, D_2O–CD_3OD, *J* in Hz) and ^{13}C NMR (125 MHz, D_2O–CD_3OD) spectroscopic data for compounds 3 and 4.

No.	3		4	
	δ_H (*J* in Hz)	δ_C	δ_H (*J* in Hz)	δ_C
1	-	44.5	-	41.2
2	1.25, m, 1.93, m	34.6	3.14, d, (9.45)	82.3 (−2.3)※
3	1.70, m, 1.93, m	30.2	3.70, m	82.6 (+8.8)※
4	1.69, m, 1.92, m	18.7	1.10, m, 2.07, m	41.8 (−2.7)※
5	-	125.8	1.49, m	33.6
6	-	133.3	0.63, dt, (11.50, 3.05)	52.7
7	2.32, m, 2.57, t (13.25)	28.4	1.17, m, 1.41, m	25.7
8	3.28, m	53.0	1.40, m, 1.57, m	41.6
9	-	213.8	3.74, m	69.2
10	2.30, s	30.3	1.15, d (6.26)	23.1
11	1.03, s	17.6	0.76, s	15.0
12	3.72, d (9.09)	91.0	1.00, s	26.4
13	1.53, s	17.4	0.94, d (6.17)	20.9
1'	4.25, d (7.65)	103.6	4.56, d (7.88)	104.6
2'	3.17, m	73.8	3.26, t (8.23, 9.03)	74.8
3'	3.20−3.42, m (overlap)	76.4	3.45, t (8.83, 9.03)	77.1
4'	3.20−3.42, m (overlap)	69.8	3.35, m	70.8
5'	3.20−3.42, m (overlap)	75.1	3.37, m	77.0
6'	3.66, m, 4.09, d (10.55)	68.0	3.69, m, 3.87, d (12.10)	61.9
1"	4.29, d (7.46)	103.0		
2"	3.20−3.42, m (overlap)	73.7		
3"	3.20−3.42, m (overlap)	76.4		
4"	3.20−3.42, m (overlap)	70.1		
5"	3.20−3.42, m (overlap)	76.4		
6"	3.67, m, 3.86, d (11.74)	61.3		

※: $\Delta\delta_{C(4\text{-}4c)}$

The relative configuration of **3** was deduced from the analysis of its coupling constants and the Nuclear Overhauser Effect Spectroscopy (NOESY) spectrum. A notable NOESY correlation between H-8 (δ_H 3.28) and H_3-11 (δ_H 1.03) indicated that H-8 and H_3-11 were axially oriented and assigned as *β*-oriented. The significant coupling constant observed between H-8/H-12 (*J* = 9.20 Hz) confirmed that H-12 was positioned on the opposite face, leading to its assignment as *α*-oriented. To determine the absolute configuration of **3**, we employed electronic circular dichroism (ECD) calculations. ECD is recognized as a powerful and effective method for confirming the absolute configuration of natural products [18]. The absolute configuration of **3** was ultimately established as 1*S*, 8*R*, 12*S* by comparing the calculated and experimental ECD spectra (Fig. 9). Furthermore, the coupling constants observed for the anomeric proton H-1' (δ_H 4.25) and H-1" (δ_H 4.29) in the ^{1}H NMR spectrum of **3** (*J* = 7.65 Hz and 7.46 Hz, respectively) indicated the presence of *β*-glucoside linkages in the megastigmane aglycone. Therefore, the complete structure of **3** was confirmed (Fig. 1).

Compound **4**, $[\alpha]_D^{25}$ −7.00 (*c* 0.06, CH_3OH), was obtained as a white powder (MeOH). Its molecular formula was determined as $C_{19}H_{36}O_8$, as indicated by positive HR-ESI-MS data at *m/z* 415.2302 ($[M + Na]^+$, Calcd. 415.2302), suggesting two degrees of unsaturation.

The comprehensive analysis of the 1D NMR spectra of **4** (Table 2) revealed 19 carbon signals. These signals were classified as four methyl groups, four methylene groups (including one hydroxyl methylene at δ_C 61.9), ten methine groups (including five hydroxyl methines at δ_C 70.8, 77.0, 74.8, 82.3, and 69.2 and three oxygenated methines at δ_C 77.1, 104.6 and 82.6), and one quaternary carbon. Detailed analyses of NMR spectra suggested that **4** contains a megastigmane unit and a glucose unit.

The planar structure of **4** was determined through analyses of ^{1}H-^{1}H COSY and HMBC spectra (Fig. 6). Extende ^{1}H-^{1}H COSY correlations of H-2/H-3/H_2-4/H-5/H-6(H_3-13)/H_2-7/H_2-8/H-9/H_3-10, in conjunction with the HMBCs of H_3-11/C-1, C-2 and C-6 and H_3-12/C-1, C-2 and C-6 illustrated that the megastigmane unit should be an ionol moiety. The anomeric proton signal at δ_H 4.56 (H-1') correlated with the carbon signals at δ_C 82.6 (C-3), suggesting the attachment of the glucose unit at C-3. Consequently, the planar structure of **4** was established, as illustrated in Fig. 1.

The coupling constant of the anomeric proton at δ_H 4.56 (*J* = 7.88 Hz) in compound **4** confirmed the *β*-configuration of the glucoside. Acid hydrolysis of **4** using hydrochloric acid yielded an aglycone, designated as **4c**, and the ^{13}C NMR chemical shifts of **4c** were compared with those of the aglycone part of **4** (Table 2). Notably, C-2 showed an upfield shift of 2.3 ppm, whereas C-4 showed a shift of 2.7 ppm. According to the glycosylation shift rules [19] of hydroxyl substitution at the *β*-carbon site of glycosides, the 2*R*, 3*R* configuration was assigned to **4**. The arbitrary assignment of H-2 in an *α*-orientation facilitated the interpretation of the H-2/H-11/H-5 NOESY correlations, implying that these protons were *α*-oriented. This finding supports the assignment of the absolute stereochemistry at C-5 as *R*. Moreover, the large coupling constant between H-5 and H-6 (*J* = 11.50 Hz) confirmed the *β*-orientation of H-6, leading to the assignment of C-6 as *S*. To determine the absolute configuration of C-9 in **4**, (*S*)- and (*R*)-MTPA esters were prepared. Significant chemical

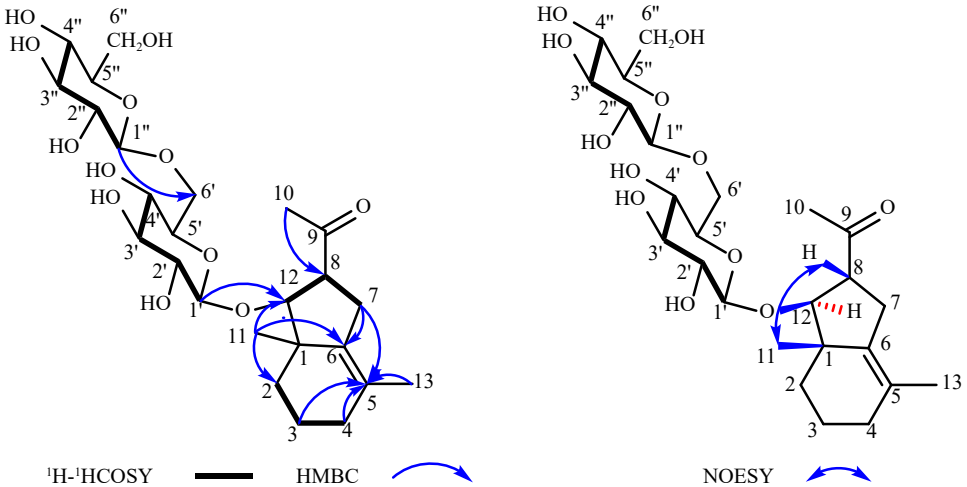

Fig. 5 Selected NMR correlations of 3.

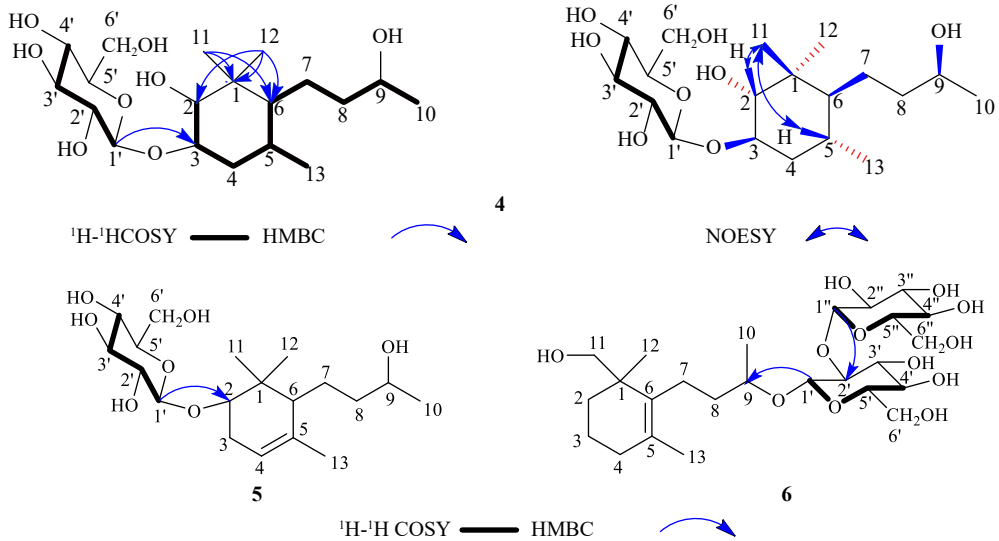

Fig. 6 Selected NMR correlations of 4–6.

shift differences ($\Delta\delta$ = $\delta_{S\text{-MTPA-ester}}$ − $\delta_{R\text{-MTPA-ester}}$) were observed for proton signals adjacent to C-9. Following the principles of Mosher's method, the absolute configuration of C-9 in **4** was determined to be *S*. Therefore, the structure of **4** was confirmed as 2*R*, 3*R*, 5*R*, 6*S*, 9*S*, as depicted in Fig. 1.

Compound **5**, $[\alpha]_D^{25}$ −5.714 (*c* 0.08, CH_3OH), was obtained as a white powder (MeOH). Its molecular formula was determined as $C_{19}H_{34}O_7$, as indicated by positive HR-ESI-MS data at *m/z* 397.2196 ($[M + Na]^+$, Calcd. 397.2197), suggesting three degrees of unsaturation.

The NMR data of **5** (Table 3) displayed similarities to those of **4**. The notable difference was the presence of a trisubstituted double bond in **5** at C-4 (δ_C 118.2) and C-5 (δ_C 137.4), in contrast to the high field carbon signals of **4**. Another difference was the shift of the signal of C-3 from the low field δ_C 82.6 to the high field δ_C 27.7, indicating that in **5**, the glucose unit was attached to C-2 instead of C-3, which was further confirmed by the HMBCs of H-1' (δ_H 4.36) with C-2 (δ_C 81.3) (Fig. 6). The *β*-configuration of **5** was determined based on the large coupling constant (δ_H 4.36, *J* = 7.93 Hz) of the anomeric proton. The absolute configuration of C-2 in **5** was determined using *β*-D-glucopyranosylation-induced chemical shifts [20], applicable to *β*-D-glucosides of secondary alcohols, especially isoprenoid-*β*-D-glucopyranosides, having at least one equatorial alkyl substituent on one of its *β*-carbons. In this method, the C-1' resonance of glucosides of *S*-alcohols is deshielded, appearing at δ_C 106.4 ± 0.5 ppm, while in *R*-alcohols, it appears in a relatively upfield region, δ_C 101.6 ± 0.9 ppm. Since the C-1' resonance in **5** appeared at δ_C 100.5 ppm, the absolute configuration of C-2 was determined to be *R*. The stereochemistry at C-6 was confirmed as 6*S* by the fact that the CD spectrum showed a positive extreme at 246 nm [$\Delta\varepsilon$ +2.67] [21]. Finally, the absolute configuration of C-9 in **5** was assigned as 9*S* by Mosher's method. Its absolute configuration was determined to be 2*R*, 6*S*, 9*S* based on the comparison of the calculated and experimental ECD spectra (Fig. 9). Therefore, the structure of **5** was established, as shown in Fig. 1.

Table 3 ^{1}H NMR (500 MHz, D_2O–CD_3OD, *J* in Hz) and ^{13}C NMR (125 MHz, D_2O–CD_3OD) spectroscopic data for compounds 5 and 6.

No.	5		6	
	δ_H (*J* in Hz)	δ_C	δ_H (*J* in Hz)	δ_C
1	-	36.9	-	39.9
2	3.57, dd (2.46, 5.40)	81.3	1.26, m, 1.78, m	33.2
3	2.02, m, 2.27, d, (17.65)	27.7	1.56, m, 1.61, m	18.7
4	5.29, br s	118.2	1.93, m, 1.93, m	32.2
5	-	137.4	-	130.0
6	1.65, m	49.7	-	133.9
7	1.33, m, 1.66, m	24.2	2.04, m, 2.19, m	23.7
8	1.42, m, 1.67, m	40.5	1.54, m, 1.63, m	36.3
9	3.74, m	68.0	3.85, m	77.5
10	1.17, d (6.20)	22.1	1.28, d (6.34)	20.3
11	0.86, s	16.6	3.31, m, 3.50, m	67.8
12	1.00, s	25.2	0.98, s	22.5
13	1.69, s	21.7	1.65, s	19.2
1'	4.36, d (7.93)	100.5	4.47, d (7.74)	101.1
2'	3.21–3.33, m (overlap)	73.3	3.21–3.60, m (overlap)	80.1
3'	3.42, t (8.60, 8.99)	76.2	3.21–3.60, m (overlap)	77.1
4'	3.21–3.33, m (overlap)	70.0	3.21–3.60, m (overlap)	70.0
5'	3.21–3.33, m (overlap)	76.0	3.21–3.60, m (overlap)	76.4
6'	3.68, dd (12.14, 5.31), 3.85, dd (12.41, 1.88)	61.0	3.66, m, 3.86, m	61.3
1"			4.70, d (7.86)	103.0
2"			3.21–3.60, m (overlap)	74.3
3"			3.21–3.60, m (overlap)	76.9
4"			3.21–3.60, m (overlap)	70.3
5"			3.21–3.60, m (overlap)	76.5
6"			3.61, m, 3.81, m	61.6

Compound **6**, $[\alpha]_D^{25}$ −33.00 (*c* 0.08, CH_3OH), was obtained as a white powder (MeOH). Its molecular formula was determined as $C_{25}H_{44}O_{12}$, as indicated by positive HRESIMS at *m/z* 559.2715 ($[M + Na]^+$, Calcd. 559.2725), suggesting four degrees of unsaturation.

The ^{13}C NMR spectrum of **6** (Table 3) revealed the presence of two hexoses, including two anomeric carbons at δ_C 101.1 (C-1') and δ_C 103.0 (C-1"), along with ten other carbons at δ_C 61.3–80.1. Apart from the glucose unit, the NMR data of **6** closely resembled those of **4**. The shift in signals of C-5 and C-6 to lower field (C-5 δ_C 130.0, C-6 δ_C 133.9) indicated the formation of a double bond group. In addition, the less shielded carbon signal at C-11 (δ_C 67.8) and the more shielded signals at C-2 and C-3 suggested that C-2 and C-3 were not linked to the oxygen group, while C-11 was related to the hydroxyl group or glucose unit, which could be inferred from the HMBC of H-1' (δ_H 4.47, *J* = 7.74 Hz) with C-9 (δ_C 77.5). According to the literature [22] and glycosylation-induced chemical shifts [19], the 9*S*-configuration was suggested for **6**. By comparing the calculated and experimental ECD spectra (Fig. 9), the absolute configuration of **6** was confirmed as 1*S*, 9*S*. Another anomeric proton signal at δ_H 4.70 (H-1") correlated with the carbon signal at δ_C 80.1 (C-2'), indicating that the second glucose was located at C-2'. Both glucose units were determined to be in the *β*-configuration, as evidenced by their large coupling constants (H-1', δ_H 4.47, *J* = 7.74 Hz, H-1", δ_H 4.70, *J* = 7.86 Hz). The structure of **6** was finally established unambiguously (Fig. 1).

Compound **7**, $[\alpha]_D^{25}$ +8.00 (*c* 0.07, CH_3OH), was obtained as a white powder (MeOH). Its molecular formula was determined as $C_{21}H_{30}O_9$, as indicated by positive HR-ESI-MS at *m/z* 449.1772 ($[M + Na]^+$, Calcd. 449.1782), suggesting seven degrees of unsaturation.

The ^{1}H, ^{13}C and DEPT NMR spectra of **7** (Table 4) identified 21 carbon signals as two methyls, five methylenes (including one hydroxyl methylene at δ_C 60.9 and one oxygenated methylene at δ_C 65.9), ten methines (including four hydroxyl methines at δ_C 69.8, 76.1, 73.3 and 81.9, and two oxygenated methines at δ_C 76.2 and 102.0, and two sp^2 carbons at δ_C 150.1 and 152.2), and four quaternary carbons (including two sp^2 carbons at δ_C 134.7 and 133.7, and one ketonic carbonyl carbon at δ_C 199.9, and one ester carbonyls at δ_C 174.8). Among them, a glucose unit (δ_C 102.0, 73.3, 76.1, 69.8, 76.2, 60.9) and an *α*,*β*-unsaturated carbonyl group (δ_C 199.9, 134.7, 150.1) were observed. ^{1}H NMR data exhibited two trisubstituted olefinic protons (δ_H 7.29, δ_H 7.46).

The structure of **7** was further elucidated by ^{1}H-^{1}H COSY and HMBC analysis, as depicted in Fig. 7. The ^{1}H-^{1}H COSY spectrum facilitated the identification of two long proton-bearing structural fragments: H_2-1/H-6/H_2-5/H-4 and H-8/H-9/H_2-10/H-11/H_3-12(H_3-15), represented by bold bonds in the figure. The HMBC correlations of H-1 (δ_H 2.74, 2.64) with C-2 (δ_C 199.9) illustrated that the fragment (H_2-1/H-6/H_2-5/H-4) and the *α*,*β*-unsaturated carbonyl group (C-2/C-3/C-4) constituted a hexane ring. Meanwhile, C-13 (δ_C 65.9) connected to C-3 on the hexane ring, as evidenced by the HMBCs of H_2-13 (δ_H 4.32, 4.48) with C-2 (δ_C 199.9), C-3 (δ_C 134.7) and C-4 (δ_C 150.1). **7** also featured a five-membered unsaturated lactone ring according to the remaining three degrees of unsaturation and the HMBC of H-8 (δ_H 7.46) with C-14 (δ_C 174.8). Furthermore, the HMBC of H_2-5 (δ_H 2.59, 2.80) with C-7 (δ_C 133.7) indicated that the hexane ring was connected to the lactone ring at C-6 and C-7. The

Table 4 ^{1}H NMR (500 MHz, D_2O–CD_3OD or CD_3OD, *J* in Hz) and ^{13}C NMR (125 MHz, D_2O–CD_3OD or CD_3OD) spectroscopic data for compounds 7 and 7a.

No.	7 (D_2O–CD_3OD)		7a (CD_3OD)	
	δ_H (*J* in Hz)	δ_C	δ_H (*J* in Hz)	δ_C
1	2.64, m, 2.74, m	41.2	7.22, dd (1.60, 7.80)	119.2
2	-	199.9	7.09, d (7.80)	131.9
3	-	134.7	-	127.1
4	7.29, m	150.1	-	156.6
5	2.59, m, 2.80, m	29.7	7.33, d (1.60)	114.0
6	3.16, m	31.5	-	129.7
7	-	133.7	-	131.7
8	7.46, m	152.2	7.76, d (1.80)	150.6
9	5.16, m	81.9	5.15, td (1.80, 4.50, 9.10)	81.2
10	1.46, m, 1.62, m	41.4	1.52, m, 1.67, m	43.6
11	1.79, m	24.9	1.91, m	26.6
12	0.96, m	21.4	1.03, d (6.86)	22.6
13	4.32, d (12.68), 4.48, d (12.57)	65.9	2.19, s	16.1
14	-	174.8	-	174.2
15	0.96, m	22.3	1.01, d (6.86)	23.5
1'	4.39, d (7.80)	102.0		
2'	3.20–3.45, m (overlap)	73.3		
3'	3.20–3.45, m (overlap)	76.2		
4'	3.20–3.45, m (overlap)	69.8		
5'	3.20–3.45, m (overlap)	76.1		
6'	3.68, m, 3.86, m	60.9		

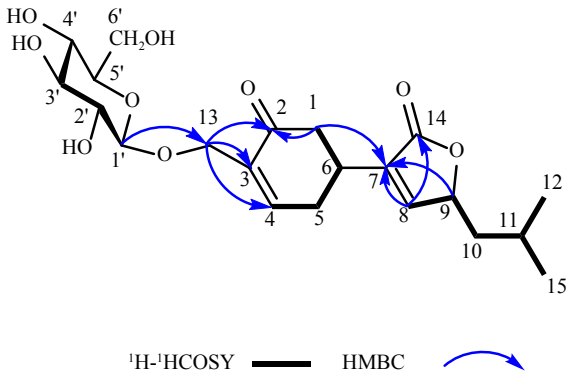

Fig. 7 Selected NMR correlations of 7.

placement of the glucose moiety at C-13 was confirmed by correlations between the proton signal at δ_H 4.39 (H-1') and the carbon signal at δ_C 65.9 (C-13). Consequently, the planar structure of **7** was established, as shown in Fig. 1.

The aglycone derived from compound **7**, referred to as **7a**, was obtained through hydrolysis with hydrochloric acid. Its structure was identified by comparing its NMR chemical shifts with those of **7**. The primary differences in NMR data between **7** and **7a** were observed in the signals from C-1 to C-6, which shifted from a hexane ring in **7** to a benzene ring in **7a** (Table 4). To determine the absolute configuration of **7a**, a suitable crystal of **7a** was obtained and subjected to single-crystal X-ray diffraction analysis using the anomalous scattering of Cu-Kα radiation. The final refinement of the given coordinate resulted in a Flack parameter of 0.03(15), which allowed for the unambiguous assignment of the absolute configuration of **7** and **7a** as 9*R* (Fig. 8). The absolute configuration of **7** was further assigned as 6*S*, 9*R* based on the good qualitative agreement between the experimental and calculated ECD spectra (Fig. 9). Additionally, the presence of an anomeric proton signal at 4.39 (*J* = 7.80 Hz) indicated the presence of a *β*-glucoside in the structure. Thus, the structure of the **7** was defined, as shown in Fig. 1.

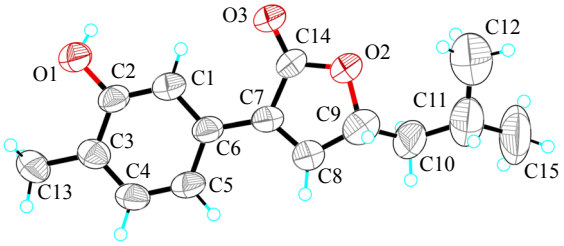

Fig. 8 X-ray crystallographic structure of 7a.

To assess the potential bioactivity and toxicity of the isolated compounds for clinical applications, we conducted a cytotoxicity evaluation. Following the methodologies outlined in previous studies [23, 24], all isolated compounds were evaluated for cytotoxicity against three human cancer cell lines, including liver cancer Hep-3B, colon cancer HCT-116, and breast cancer MCF-7 cells, as well as the immortalized noncancerous human umbilical vein endothelial cells (HUVEC). The results indicated that **1**–**7a** exhibited no significant cytotoxicity (IC_{50} > 100 μmol·L^{-1}).

Experimental

General experimental procedures

Column chromatography (CC): Silica gel (200–300 mesh; Marine Chemical Factory, Qingdao, China), RP-C_{18} gel (40–63 μm; Daiso Co., Japan), and Sephadex LH-20 (Pharmacia Fine Chemicals, Piscataway, NJ, USA) were used for various CC separations. TLC: Silica gel plates were employed for TLC, and the visualization of the TLC plates was achieved by spraying with 10% H_2SO_4 in EtOH. Ultra-performance liquid chromatography (UPLC): UPLC was performed on the ACQUITY H-Class system (Waters Technologies, US) with a Zorbax SB-C_{18} (1.8 μm, 2.1 mm × 100 mm) column. NMR spectra: NMR spectra were recorded on Bruker Avance III-500 and Bruker Avance III-600 spectro-

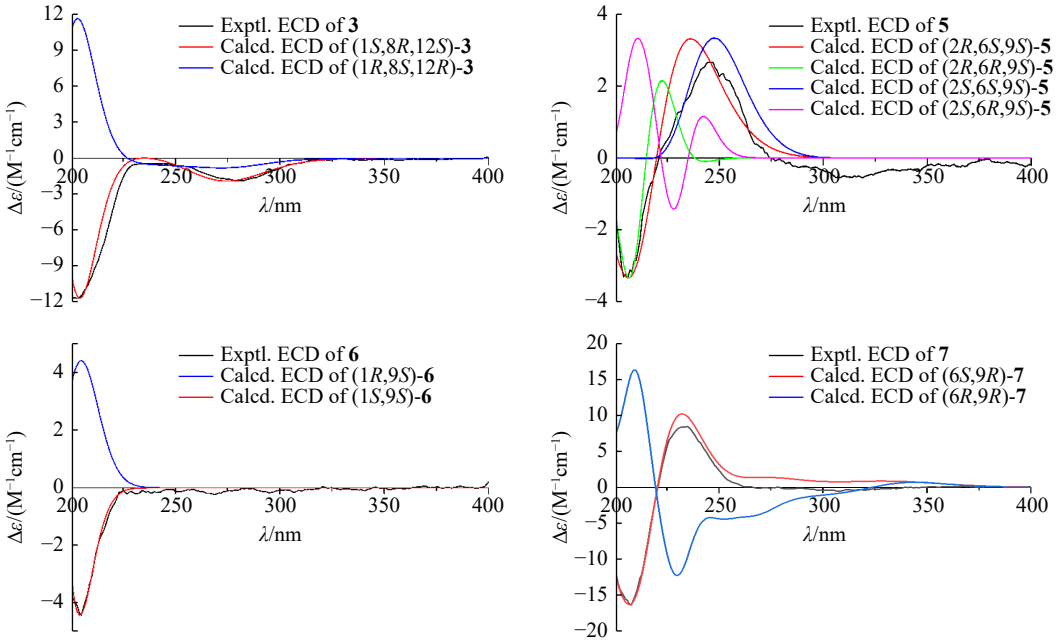

Fig. 9 Experimental and calculated ECD spectra of 3, 5−7.

meters (Bruker, Switzerland). MS: Agilent MSD-Trap-XCT was used for ESI-MS, and Agilent-6520 Q-TOF mass spectrometer was utilized for HR-ESI-MS. CD spectra: Measurements were conducted using a Brighttime Chirascan (Applied Photophysics Ltd., UK). Optical rotation: Optical rotation was measured using a Rudolph Autopo V (Rudolph Research Analytical, Hackettstown, NJ).

The leaves of G. biloba

The *G. biloba* leaves used in this study were collected from Zhejiang Province, China, in March 2018. Their identification was expertly conducted by Professor HUANG Baokang of the Department of Pharmacognosy, School of Pharmacy, at the Naval Military Medical University. For reference and further research purposes, a voucher specimen (No. 201803-GA) has been deposited at the Department of Pharmacognosy, Naval Medical University, China.

Extraction and isolation

The dried *G. biloba* leaves (50 kg) underwent maceration with 70% ethanol overnight at room temperature (3 × 1000 L). Post-solvent removal, the resulting ethanol extract (1.8 kg) was dissolved in water and subjected to silica gel chromatography (200−300 mesh) using EtOAc/MeOH (100 ∶ 0 to 0 ∶ 100), yielding nine fractions (Frs. 1−9). Fr. 8 (88.7 g) was applied to silica gel (200−300 mesh) (EtOAc/MeOH, 80 ∶ 20 to 20 ∶ 80) to obtain 24 subfractions (Frs. 8.1−8.24). Fr. 8.23 (7.6 g) was purified by ODS CC ($MeOH/H_2O$, 10 ∶ 90 to 30 ∶ 70) to yield six subfractions (Frs. 8.23.1–8.23.6). From Fr. 8.23.1 (0.9 g), Sephadex LH-20 CC ($MeOH/H_2O$, 20 ∶ 80) isolated compound **2** (35.2 mg). Fr. 8.23.3 (1.3 g) was purified by preparative RP-C_{18} HPLC ($MeOH/H_2O$, 24 ∶ 76) to yield compounds **1** (46.3 mg) and **4** (50.7 mg). Subsequently, subfraction Fr. 8.9 (10.5 g) underwent further purification by ODS CC ($MeOH/H_2O$, 10 ∶ 90 to 30 ∶ 70), yielding subfractions (Frs. 8.9.1–8.9.4). Fr. 8.9.2 (2.4 g) was then purified by preparative RP-C_{18} HPLC ($MeOH/H_2O$, 18 ∶ 82 to 28 ∶ 72), yielding compounds **3** (17.6 mg) and **6** (14.5 mg). After that, Fr. 8.17 (9.7 g) was further purified by Sephadex LH-20 CC ($MeOH/H_2O$, 20 ∶ 80 to 50 ∶ 50) followed by ODS CC ($MeOH/H_2O$, 25 ∶ 75 to 40 ∶ 60) to produce compounds **5** (11.7 mg) and **7** (190.7 mg). Finally, the aglycone **7a** (20.9 mg) was obtained by acid hydrolysis of **7** (80 mg). In summary, this extraction and isolation process successfully yielded compounds **1** (46.3 mg), **2** (35.2 mg), **3** (17.6 mg), **4** (50.7 mg), **5** (11.7 mg), **6** (14.5 mg), **7** (190.7 mg), and **7a** (20.9 mg).

Spectral data of compounds 1−7

Compound **1**: White needle crystals; ^1H and ^{13}C NMR data (Table 1); positive HR-ESI-MS *m/z* 349.1264 ($[M + Na]^+$, Calcd. 349.1258). CCDC: 2090818.

Compound **2**: White needle crystals; ^1H and ^{13}C NMR data (Table 1); positive HR-ESI-MS *m/z* 349.1257 ($[M + Na]^+$, Calcd. 349.1258). CCDC: 2131792.

Compound **3**: White powder; $[\alpha]_D^{25}$ −47.33 (*c* 0.08, CH_3OH); ^1H and ^{13}C NMR data (Table 2); positive HR-ESI-MS *m/z* 555.2411 ($[M + Na]^+$, Calcd. 555.2412).

Compound **4**: White powder; $[\alpha]_D^{25}$ −7.00 (*c* 0.06, CH_3OH); ^1H and ^{13}C NMR data (Table 2); positive HR-ESI-MS *m/z* 415.2302 ($[M + Na]^+$, Calcd. 415.2302).

Compound **5**: White powder; $[\alpha]_D^{25}$ −5.714 (*c* 0.08, CH_3OH); ^1H and ^{13}C NMR data (Table 3); positive HR-ESI-MS *m/z* 397.2196 ($[M + Na]^+$, Calcd. 397.2197).

Compound **6**: White powder; $[\alpha]_D^{25}$ −33.00 (*c* 0.08, CH_3OH); ^1H and ^{13}C NMR data (Table 3); positive HR-ESI-MS *m/z* 559.2715 ($[M + Na]^+$, Calcd. 559.2725).

Compound **7**: White powder; $[\alpha]_D^{25}$ +8.00 (*c* 0.07,

CH_3OH); ^1H and ^{13}C NMR data (Table 4); positive HR-ESI-MS *m/z* 449.1772 ($[M + Na]^+$, Calcd. 449.1782).

Compound **7a**: White needle crystals; $[\alpha]_D^{25}$ +14.72 (*c* 0.06, CH_3OH); ^1H and ^{13}C NMR data (Table 4); positive HR-ESI-MS *m/z* 247.1326 ($[M + H]^+$, Calcd. 247.1329). CCDC: 2183880.

*(R)- and (S)-MTPA esters of compounds **4** and **5***

To each compound **4** and **5** (each 1.5 mg) in pyridine-d_5 (130 μL) was separately added (*R*)-(−)-MTPA (5 μL) and (*S*)-(+)-MTPA (5 μL) at room temperature, followed by stirring at 40 °C for 8 h, and each reaction mixture was transferred into a 1.7 mm NMR tube.

(*R*)-MTPA ester of **4**: ^1H NMR (pyridine-d_5, 500 MHz) *δ*: 1.35 (3H, m, H_3-10), 0.85 (3H, m, H_3-11), 0.98 (3H, m, H_3-13), 1.26 (3H, s, H_3-12), 1.41 (1H, m, H-4a).

(*S*)-MTPA ester of **4**: ^1H NMR (pyridine-d_5, 500 MHz) *δ*: 1.30 (3H, m, H_3-10), 0.68 (3H, m, H_3-11), 0.90 (3H, m, H_3-13), 1.10 (3H, m, H_3-12), 1.40 (1H, m, H-4a).

(*R*)-MTPA ester of **5**: ^1H NMR (pyridine-d_5, 500 MHz) *δ*: 1.32 (d, *J* = 6.15 Hz, H-10), 0.92 (3H, s, H_3-11), 1.04 (3H, m, H_3-12), 1.68 (3H, s, H_3-13).

(*S*)-MTPA ester of **5**: ^1H NMR (pyridine-d_5, 500 MHz) *δ*: 1.29 (d, *J* = 6.15 Hz, H-10), 0.89 (3H, s, H_3-11), 1.02 (3H, m, H_3-12), 1.65 (3H, s, H_3-13).

X-ray crystallography

Crystallographic analyses for compounds **1**, **2**, and **7a** were conducted on a Bruker APEX-II CCD detector using graphite-monochromated Cu-Kα radiation. Their structures were solved by direct methods (SHELXS-97) and refined on F^2 with full-matrix least-squares calculations. The crystallographic data of **1**, **2**, and **7a** have been deposited in the Cambridge Crystallographic Data Centre, with the respective numbers CCDC 2090818, 2131792, and 2183880. These data are available free of charge *via* http://www.ccdc.cam.ac.uk/data request/cif.

Crystallographic data for compound **1** ($C_{16}H_{22}O_7$): M = 326.33, size: 0.18 × 0.15 × 0.12 mm^3, orthorhombic space group: *P* 21, *a* = 8.0375 (4) Å, *b* = 6.1509 (3) Å, *c* = 15.7797 (8) Å, *V* = 778.44 (7) $Å^3$, *T* = 293 (2) K, *Z* = 2, *D* = 1.392 $mg·m^{-3}$, *λ*(Cu-Kα) = 1.541 78 Å, *F*(000) = 348, reflections collected/unique: 12 573/2692 [$R_{(int)}$ = 0.0314], *h* (−9/8), *k* (−7/6), *l* (−18/18), Final *R* indices: R_1 = 0.0289 and wR_2 = 0.0782 [$I > 2\sigma(I)$], R_1 = 0.0290 and wR_2 = 0.0783 (all data), Goodness of Fit (GOF) = 1.050, largest diff. peak/hole: 0.154/−0.133 $eÅ^{-3}$, and absolute structure parameter: 0.02 (3).

Crystallographic data for compound **2** ($C_{16}H_{22}O_7$): M = 326.33, size: 0.07 × 0.07 × 0.05 mm^3, orthorhombic space group: *P* 1211, *a* = 9.843 30 (10) Å, *b* = 6.294 60 (10) Å, *c* = 13.3181 (2) Å, *V* = 769.396 (19) $Å^3$, *T* = 213.00 K, *Z* = 2, *D* = 1.409 $mg·m^{-3}$, *λ*(Cu-Kα) = 1.341 39 Å, *F*(000) = 348, reflections collected/unique 10 401/2894 [$R_{(int)}$ = 0.0360], *h* (−12/12), *k* (−7/7), *l* (−16/16), Final *R* indices: R_1 = 0.0352 and wR_2 = 0.0901 [$I > 2\sigma(I)$], R_1 = 0.0365 and wR_2 = 0.0912 (all data), GOF = 1.038, largest diff. peak/hole: 0.482/−0.430 $eÅ^{-3}$, and absolute structure parameter: 0.06 (7).

Crystallographic data for compound **7a** ($C_{15}H_{18}O_3$): M = 246.29, size: 0.07 × 0.07 × 0.05 mm^3, orthorhombic space group: *P* 1211, *a* = 9.7923 (3) Å, *b* = 11.6114 (3) Å, *c* = 11.9415 (3) Å, *V* = 1354.25 (6) $Å^3$, *T* = 213.00 K, *Z* = 4, *D* = 1.208 $mg·m^{-3}$, *λ*(Cu-Kα) = 1.341 39 Å, *F*(000) = 528, reflections collected/unique: 16 177/5106 [$R_{(int)}$ = 0.0492], *h* (−11/11), *k* (−13/14), *l* (−14/14), Final *R* indices R_1 = 0.0785 and wR_2 = 0.1912 [$I > 2\sigma(I)$], R_1 = 0.1244 and wR_2 = 0.2245 (all data), GOF = 1.021, largest diff. peak/hole: 0.511/−0.315 $eÅ^{-3}$, and absolute structure parameter: 0.03 (15).

Cell culture and cytotoxicity assay

The cytotoxicity assay involved three human cancer cell lines: Hep-3B (liver cancer), HCT-116 (colon cancer), and MCF-7 (breast cancer), as well as one noncancerous human umbilical vein endothelial cell line (HUVEC). All cells were purchased from the Shanghai Institute of Biochemistry and Cell Biology, Chinese Academy of Sciences (Shanghai, China) and cultured in DMEM or McCoy's 5A in a humidified atmosphere containing 5% CO_2 at 37 °C.

All the isolated compounds were dissolved in dimethyl sulfoxide (DMSO) and freshly prepared each time before use. Then, 100 μL of adherent cells were seeded into each well of the 96-well culture plates and allowed to adhere for 12 h before the addition of the test compounds. Suspended cells were seeded just before the addition of the drug at an initial density of 5 × 10^3 $cells·mL^{-1}$. The cells were then treated with 100 μL of culture medium containing compounds at gradient concentrations for 48 h. Then, cell viability was determined *via* the Cell Counting Kit-8 assay (CCK-8, TOP- Science, China). Post-treatment, 10 μL of CCK-8 solution was added to each well, followed by incubation at 37 °C for 30 min. The optical density (OD) at 450 nm was spectrophotometrically measured using a microplate reader (BioTek Instruments, Inc.).

Conclusion

In conclusion, two novel phenylbutenoids and five previously unidentified terpene glycosides have been isolated from *G. biloba* leaves, and their structures have been elucidated. The findings of this study not only lay a solid scientific foundation for the rational development and utilization of this plant but also provide valuable chemical insights that could inform future studies investigating the pharmacological potential and therapeutic applications of these newly discovered compounds.

Acknowledgement

We are grateful to Dr. LU Lu for carrying out the NMR experiments.

References

[1] Banin RM, Hirata BKS, Andrade IS, *et al*. Beneficial effects of *Ginkgo biloba* extract on insulin signaling cascade, dyslipidemia, and body adiposity of diet-induced obese rats [J]. *Braz*

J Med Biol Res, 2014, **47**(9): 780-788.
[2] Eisvand F, Razavi BM, Hosseinzadeh H. The effects of *Ginkgo biloba* on metabolic syndrome: a review [J]. *Phytother Res*, 2020, **34**(8): 1798-1811.
[3] Singh SK, Srivastav S, Castellani RJ, *et al*. Neuroprotective and antioxidant effect of *Ginkgo biloba* extract against AD and other neurological disorders [J]. *Neurotherapeutics*, 2019, **16**(3): 666-674.
[4] Dong W, Zhao S, Wen S, *et al*. A preclinical randomized controlled study of ischemia treated with *Ginkgo biloba* extracts: are complex components beneficial for treating acute stroke [J]. *Curr Res Transl Med*, 2020, **68**(4): 197-203.
[5] Ji H, Zhou X, Wei W, *et al*. *Ginkgol biloba* extract as an adjunctive treatment for ischemic stroke: a systematic review and meta-analysis of randomized clinical trials [J]. *Medicine*, 2020, **99**(2): e18568.
[6] Liu L, Wang Y, Zhang J, *et al*. Advances in the chemical constituents and chemical analysis of *Ginkgo biloba* leaf, extract, and phytopharmaceuticals [J]. *J Pharm Biomed Anal*, 2021, **193**: 113704.
[7] Wang X, Gong X, Zhang H, *et al*. *In vitro* anti-aging activities of *Ginkgo biloba* leaf extract and its chemical constituents [J]. *Food Sci Technol*, 2020, **40**: 476-482.
[8] Dong HL, Lin S, Wu QL, *et al*. A new bilobalide isomer and two *cis*-coumaroylated flavonol glycosides from *Ginkgo biloba* leaves [J]. *Fitoterapia*, 2020, **142**: 104516.
[9] Yu H, Dong LH, Zhang Y, *et al*. A network pharmacology-based strategy for predicting the protective mechanism of *Ginkgo biloba* on damaged retinal ganglion cells [J]. *Chin J Nat Med*, 2022, **20**(1): 54-66.
[10] Okhti ZA, Abdalah ME, Hanna DB. Phytochemical structure and biological effect of *Ginkgo biloba* leaves: a review [J]. *Int J Pharm Res*, 2021, 13(2): 1138-1143.
[11] Akiba S, Chiba M, Mukaida Y, *et al*. The leaf extract of *Ginkgo biloba* L. suppresses oxidized LDL-stimulated fibronectin production through an antioxidant action in rat mesangial cells [J]. *Br J Pharmacol*, 2004, **142**(3): 419-424.
[12] Mashayekh A, Pham DL, Yousem DM, *et al*. Effects of *Ginkgo biloba* on cerebral blood flow assessed by quantitative MR perfusion imaging: a pilot study [J]. *Neuroradiology*, 2011, **53**(3): 185-191.
[13] Shinozuka K, Umegaki K, Kubota Y, *et al*. Feeding of *Ginkgo biloba* extract (GBE) enhances gene expression of hepatic cytochrome P-450 and attenuates the hypotensive effect of nicardipine in rats [J]. *Life Sci*, 2002, **70**(23): 2783-2792.
[14] Naik SR, Panda VS. Antioxidant and hepatoprotective effects of *Ginkgo biloba* phytosomes in carbon tetrachloride-induced liver injury in rodents [J]. *Liver Int*, 2007, **27**(3): 393-399.
[15] Cho KS, Lee IM, Sim S, *et al*. *Ginkgo biloba* extract (EGb 761®) inhibits glutamate-induced up-regulation of tissue plasminogen activator through inhibition of c-Fos translocation in rat primary cortical neurons [J]. *Phytother Res*, 2016, **30**(1): 58-65.
[16] Liu XG, Lu X, Gao W, *et al*. Structure, synthesis, biosynthesis, and activity of the characteristic compounds from *Ginkgo biloba* L. [J]. *Nat Prod Rep*, 2022, **39**: 474-511.
[17] Ude C, Schubert-Zsilavecz M, Wurglics M. *Ginkgo biloba* extracts: a review of the pharmacokinetics of the active ingredients [J]. *Clin Pharmacokinet*, 2013, **52**(9): 727-749.
[18] Wu Z, Wang Q, Fu L, *et al*. Vlasoulides A and B, a pair of neuroprotective C_{32} dimeric sesquiterpenes with a hexacyclic 5/7/5/5/(5)/7 carbon skeleton from the roots of *Vladimiria souliei* [J]. *RSC Adv*, 2021, **11**(11): 6159-6162.
[19] Seo S, Tomita Y, Tori K, *et al*. Determination of the absolute configuration of a secondary hydroxy group in a chiral secondary alcohol using glycosidation shifts in carbon-13 nuclear magnetic resonance spectroscopy [J]. *J Am Chem Soc*, 1978, **100**(11): 3331-3339.
[20] Kasai R, Suzuo M, Asakawa J, *et al*. Carbon-13 chemical shifts of isoprenoid-*β*-D-glucopyranosides and -*β*-D-mannopyranosides. Stereochemical influences of aglycones alcohols [J]. *Tetrahedron Lett*, 1977, **18**(2): 175-178.
[21] Yamano Y, Ito M. Synthesis of optically active vomifoliol and roseoside stereoisomers [J]. *Chem Pharm Bull*, 2005, **53**(5): 541-546.
[22] Yamano Y, Shimizu Y, Ito M. Stereoselective synthesis of optically active 3-hydroxy-7,8-dihydro-*β*-ionol-glucosides [J]. *Chem Pharm Bull*, 2003, **51**(7): 878-882.
[23] Shu P, Wei X, Xue Y, *et al*. Wilsonols A–L, megastigmane sesquiterpenoids from the leaves of *Cinnamomum wilsonii* [J]. *J Nat Prod*, 2013, **76**(7): 1303-1312.
[24] Wang Y, Zhao B, Ma HR, *et al*. Two new sesquiterpenoid glycosides from the leaves of *Lycium barbarum* [J]. *J Asian Nat Prod Res*, 2016, **18**(9): 871-877.

Cite this article as: SUN Zeshi, LIN Shan, WU Zhi-Li, DONG Hong-Yuan, XU Xi-Ke, LI Hui-Liang, WANG Jinxin. New phenylbutenoids and terpene glycosides from *Ginkgo biloba* leaves [J]. *Chin J Nat Med*, 2024, **22**(2): 161-170.